

Facile Synthesis of Conducting Hydrogels Based on Polyaniline Fiber and Graphene Oxide for Application in all-solid-state Supercapacitors

Guizhen Guo¹, Youyi Sun^{1,2,*}, Yibing Ma¹, Yaya Zhou¹, Zhiyuan Xiong², Yaqing Liu¹

¹ Shanxi Province Key Laboratory of Functional Nanocomposites, North University of China, Taiyuan 030051, P.R. China.

² Department of Chemical and Bio-molecular Engineering, The University of Melbourne, Victoria 3010, Australia.

*E-mail: syyi@pku.edu.cn

Received: 1 November 2018 / Accepted: 31 December 2018 / Published: 10 May 2019

A new conducting hydrogel based on graphene oxide (GO) and polyaniline (PANi) fibers was facile synthesized (denoted as GO/SA/PANi) for application in flexible all-solid-state supercapacitor device. Taking advantage of the synergistic effects of the components and synthesis strategies, the conducting hydrogels showed high mechanical stability and conductivity (16.8 S/m). Furthermore, the supercapacitor based on GO/SA/PANi exhibited high area specific capacitance (2.3 F/cm² at 0.5 mA/cm²). This study not only represents a novel conducting hydrogel for application in all-solid-state supercapacitor with high performance, but also provides a new method for enhancing capacitance and mechanical stability of conducting hydrogels.

Keywords: GO/SA/PANi; in-situ polymerization; macromolecular interaction; conducting hydrogel; supercapacitor

1. INTRODUCTION

In recent years, the flexible solid-state supercapacitor combined with exceptionally long cycle life, high power density, environmental friendliness, safety, flexibility and stability, afford a very promising option for energy storage applications [1-3]. As well-known, the development of new conducting polymer hydrogels (CPHs) is the key role to achieve flexible solid-state supercapacitors with high specific capacitance [4].

Conducting polymer hydrogels based on PANi have attracted considerable attentions due to their excellent electrical conductivity, high electrochemical activity and fast faraday effect [5-10]. At the same

time, other non-conducting polymers (eg. polyvinyl alcohol) were generally used to improve mechanical stability of conducting polymer hydrogels based on polyaniline [9-10]. Nevertheless, many of them resulted in significant drawbacks, such as poor conductivity and low capacitance. To overcome these disadvantages, the PANi fiber with high surface area was generally designed by in-situ polymerization [11-12]. In addition, GO could effectively enhance the electrochemical activity and mechanical stability of polymer hydrogels [13-15]. Although, some works have reported the synthesis of PANi/GO composites applied in supercapacitors [16-18], yet, there are few works reporting the synthesis and electrochemical properties of conducting polymer hydrogels based on PANi fiber and GO [19-21].

In this paper, a new conducting polymer hydrogel based on PANi fiber, GO and sodium alginate (SA) was prepared at room temperature by in-situ one-step polymerization. The conducting hydrogel has excellent mechanical stability and flexibility. Furthermore, it exhibited good electrochemical properties in the applied of supercapacitor devices. The proposed technique offers a novel high performance and eco-friendly electrode materials for application in flexible electrochemical energy storage.

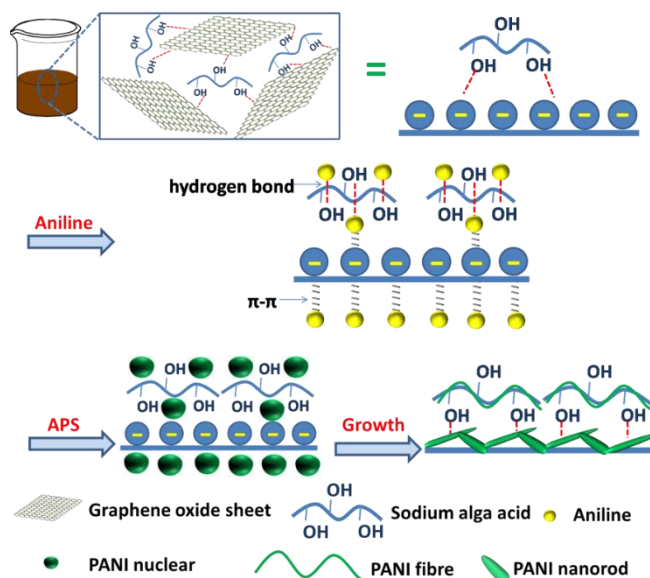
2. EXPERIMENTAL

2.1 Materials and reagents

Sodium alga acid (SA), Aniline (AN), ammonium persulfate (APS) and polyvinyl alcohol (PVA, 99% hydrolyzed, degree of polymerization 1750) were analytical grade and purchased from Shanghai Chemical Reagent Co. Graphene oxide (GO, 2.3wt%) in the form of aqueous pastes was purchased from Tangshan Jianhua Technology Co., Ltd. Carbon cloths (CC) were purchased from Nanjing MANKATE Co., Ltd., China, were utilized as current collector. Thickness and area density of original carbon cloths were 0.32 mm and 220.0 g/m², respectively. Polyester mesh (thickness: 5 μm) was purchased from Spectrum Labs, with mesh opening 10μm and opening area 2%. The reagents of HNO₃ and HCl were analytical grade and also purchased from Sinopharm Chemical Reagent Co. Ltd.

2.2 Preparation of conducting polymer hydrogels

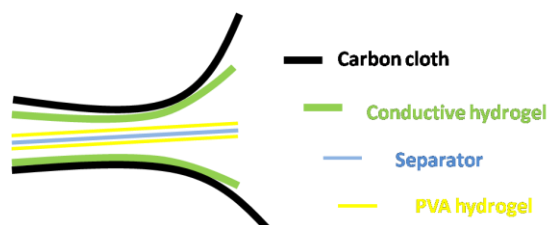
The conducting polymer hydrogels was synthesis as shown in Scheme 1. Firstly, 1.5 g GO was added to 10.0 ml deionized water and sonicated for 15.0 min in an ultrasonic bath. Secondly, 0.2 g SA was added into the GO solution, and the mixture was stirred at room temperature for 2 h. Subsequently, 0.37 g (4.0 mmol) AN was added into the above solution under stirring at room temperature for 15.0 min. And then, 0.91 g (4.0 mmol) APS was added into the above mixture under vigorous stirring at room temperature, it change to dark green colloid after about 5.0 min. After standing for 10.0 min at room temperature, a stable hydrogel was formed (denoted as GO/SA/PANi). The GO/SA/PANi hydrogel was immersed into a large amount of water for 3 days to remove inorganic impurities and excess AN. The water was changed every 12.0 h. As a control, the hydrogel without GO (denoted as SA/PANi) was prepared by the same process.



Scheme 1. Synthesis process and structure of the conducting polymer hydrogel

2.3 Fabrication of the flexible solid-state supercapacitor based on conductive hydrogel

The flexible solid-state supercapacitor based on conductive hydrogel was prepared as shown in Scheme 2. Firstly, the carbon cloth was treated by immersing in HNO_3 for 3.0 days to obtain hydrophilic carbon cloth. The above dark green colloid (ca. 3.0 g) was coated onto the hydrophilic carbon cloths (coating area of $2.0 \text{ cm} \times 2.0 \text{ cm}$). After 10.0 min, the hydrogel (thickness is about 0.5 mm) was formed on hydrophilic carbon cloths. Secondly, a piece of polyester mesh (serving as the separator) was saturated by HCl/PVA electrolyte. Two conductive hydrogel electrodes ($1.0 \text{ cm} \times 2.0 \text{ cm}$) and the polyester mesh were sandwiched together to obtain the flexible solid-state supercapacitor.



Scheme 2. Diagram of supercapacitor structure.

2.4 Characteristic measurements

The morphology of conducting hydrogels were examined by a transmission electron microscope (TEM, Tecnai G2 F30, FEI) and a scanning electron microscope (SEM, JSM-6700F) at an acceleration voltage of 5 kV. Fourier transform infrared (FT-IR) was recorded on a FT-IR spectrophotometer (Thermo Nicolet 360) from 4000 to 500 cm^{-1} at room temperature. The structure and phase of the product were identified by powder X-ray diffraction (XRD, Smartlab (3), Rigaku, Japan) with $\text{Cu K}\alpha$ radiation

diffractometer ($\lambda = 0.154\ 06\ \text{nm}$, operating voltage 35 k V, current 40 mA) over the scan range $5^\circ\text{-}60^\circ$, scanning speed of $4^\circ\ \text{min}^{-1}$. UV absorption spectrum (UV-2501, Shimadzu Co. Japan) was obtained in a range of 200 to 800 nm at room temperature. Raman spectrum was collected on a Jobin-Yvon Lab Ram HR800 Raman spectroscope equipped with a 514.5 nm laser source.

The electrical conductivity was measured via the four-probe method at room temperature by inserting the four probes into cuboid samples with the dimension of $10.0\ \text{mm}\times 30.0\ \text{mm}\times 3.0\ \text{mm}$ (RTS-8 4-point probes resistivity measurement system, Probes Tech., China). There are five samples as a group, and the average value was used as the finally electrical conductivity. Based on the data of four-point-probe instrument, the electrical conductivities of conductive hydrogels can be calculated by the following equation:

$$\delta = \frac{0.69314 \times I}{3.14 \times U \times d} \quad (1)$$

Where δ (S/m) is the electrical conductivity of electrode material, and I (mA) is the test current, U (V) is the test voltage, d (mm) is the thickness of conductive hydrogel.

2.5 Electrochemical measurements

Cyclic voltammetry (CV) and galvanostatic charge/discharge (GCD) tests were measured from -0.2 to 0.8 V. Electrochemical impedance spectroscopy (EIS) measurement was carried out in a frequency range of 0.01 Hz~100.0 kHz. All the electrochemical tests were conducted with an electrochemical workstation (CHI660E, Chenhua, Shanghai) using two-electrode system in a 1.0 M H_2SO_4 aqueous electrolyte solution at room temperature.

Based on the data of GCD, the special capacitance of electrode materials can be calculated by the following equations:

$$C_s = \frac{2I\Delta t}{s\Delta V} \quad (2)$$

$$C_m = \frac{It}{m\Delta V} \quad (3)$$

Where C_s (mF cm^{-2}) is the areal capacitance of the textile materials, and C_m (F/g) is the specific capacitance, S ($\approx 2.0\ \text{cm}^2$) is the surface area of the individual electrode, I (mA) is the discharge current, m (mg) is the mass of active material in composites, Δt (s) is the discharge time, and ΔV (V) is the potential window during the discharge process excluding IR-drop in eqn (2) and (3).

3. RESULTS AND DISCUSSION

Here, the conducting polymer hydrogels (CPHs) were prepared by a macromolecular interaction method. The PANi and SA were both key reagents for formation of hydrogels. If the PANi or SA was missed, the hydrogel would not formed as shown in Figure 1A. If the GO was missed, the hydrogel showed low mechanical stability as shown in Figure 1B. When we applied a weight of 200.0 g onto the GO/SA/PANi hydrogel, there have not any damage. As a comparison, while SA/PANi hydrogel was destroyed. This result was mainly attributed to following two reasons. Firstly, the GO was a good kind of mechanical reinforcement agent [13-14]. An effective load transferred was contributed by the strong

GO interfacial interactions. Secondly, there presented some new interactions between polar groups and hexatomic rings. The synthesis process of hydrogel was more facile comparing to previous works, for example, reaction under room temperature, short reaction time, easy process ability and low cost.

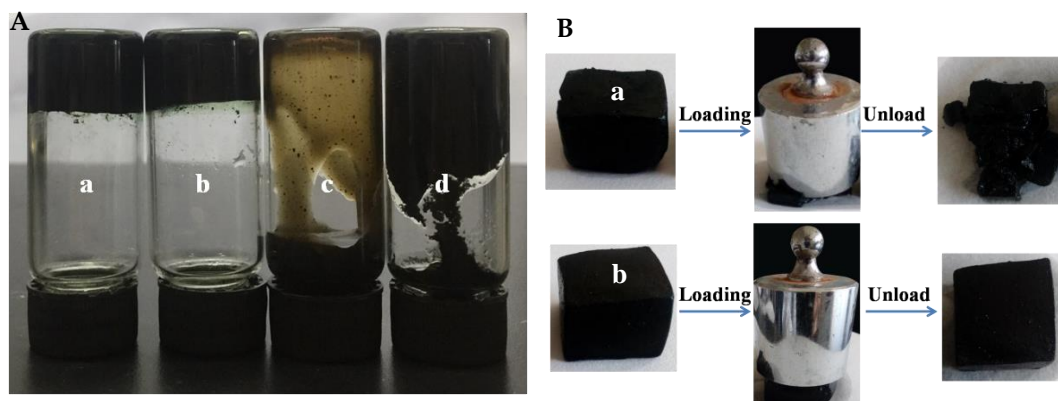


Figure 1. (A) The photographs of (a) GO/SA/PANi, (b) SA/PANi, (c) GO/SA and (d) GO/PANi. (B) Optical photograph of (a) SA/PANi and (b) GO/SA/PANi hydrogel under loading and unload.

Figure 2A shows FT-IR spectra of SA, PANi, GO, SA/PANi and GO/SA/PANi. For pure SA sample, the absorption bands at 3413.0 cm^{-1} , 2929.0 cm^{-1} and 1024.0 cm^{-1} were assigned to O-H stretching, C-H stretching and C-O-C stretching vibration of SA, respectively [11]. The two absorption bands at 1639.0 cm^{-1} and 1415.0 cm^{-1} were assigned to anti-symmetric and symmetric stretching oscillations of $-\text{COO}^-$. For pure PANi sample, the absorption bands at 3423.0 cm^{-1} , 1554.0 cm^{-1} , 1454.0 cm^{-1} , 1120.0 cm^{-1} and 715.0 cm^{-1} were assigned to N-H stretching vibration, C=C stretching vibration of quinoid, benzene rings, C-N stretching and out of plane bending vibrations of C-H of PANi, respectively [12]. For pure GO sample, the absorption bands at 1697.0 cm^{-1} , 1621.0 cm^{-1} and 3407.0 cm^{-1} were assigned to C=O, benzenoid C=C and O-H of GO, respectively [13-15]. For SA/PANi, some characteristic peaks of PANi and SA were shifted due to macromolecule interaction between PANi and SA. For example, the characteristic peak of $-\text{COO}^-$ in PANi/SA exhibited a red-shift from 1639.0 cm^{-1} to 1658.0 cm^{-1} and a weaker absorption, which was caused by the formation of ionic bonds comparing to pure SA [22]. Similarly, all characteristic bands of SA, PANi and GO presented in FT-IR spectra of GO/SA/PANi. Comparing to single GO, PANi and SA, the strength of characteristic peaks in GO/SA/PANi were weaker, and some characteristic peaks were shifted. For example, the absorption peak of C=O in the edge carboxyl group of the GO exhibited a red-shift from 1714.0 cm^{-1} to 1720.0 cm^{-1} . It was attributed to the formation of π - π interaction between PANi and GO [23]. Figure 2B shows UV-vis absorption spectra of SA, PANi, GO, SA/PANi and GO/SA/PANi. An intense absorption peak at 224.0 nm was observed in GO, corresponding to the π - π^* transition of C=C. For PANi, 228.0 nm (π - π^* transition), 321.0 nm (π - π^* transition), 404.0 nm (n - π^* transition) and a broad band at 765.0 nm (π -polar on transition) were observed in the UV-vis spectrum of PANi. Moreover, SA/PANi and GO/SA/PANi displayed similar absorption peaks to pristine PANi, indicating of the formation of GO/SA/PANi hydrogel. The absorption peaks of PANi in GO/SA/PANi hydrogel were all shifted comparing to pure PANi, such as the absorption band at 775.0 nm shift to 850.0 nm . The red-shift phenomenon was ascribed

to the enhanced π conjugation for PANi, resulting from the strong π - π interaction between PANi and SA chains or GO. Figure 2C shows Raman spectra of SA, PANi, GO, SA/PANi and GO/SA/PANi. All samples showed similar Raman peaks. The peaks at 1571.8 cm^{-1} and 1347.0 cm^{-1} were assigned to the G band and D band of GO, respectively [24-25]. The peaks at 1351.0 cm^{-1} and 1567.0 cm^{-1} were attributed to C-N stretching and C=C vibration of PANi, respectively [26-27]. At the same time, these characteristic peaks in GO/SA/PANi composites were also shifted comparing to single GO, SA and PANi. The result was also attributed to macromolecule interaction between GO, SA and PANi. The formation of GO/SA/PANi was further confirmed by XRD (Figure 2D). GO showed a sharp peak at 12.5° , corresponding to the interlayer spacing.

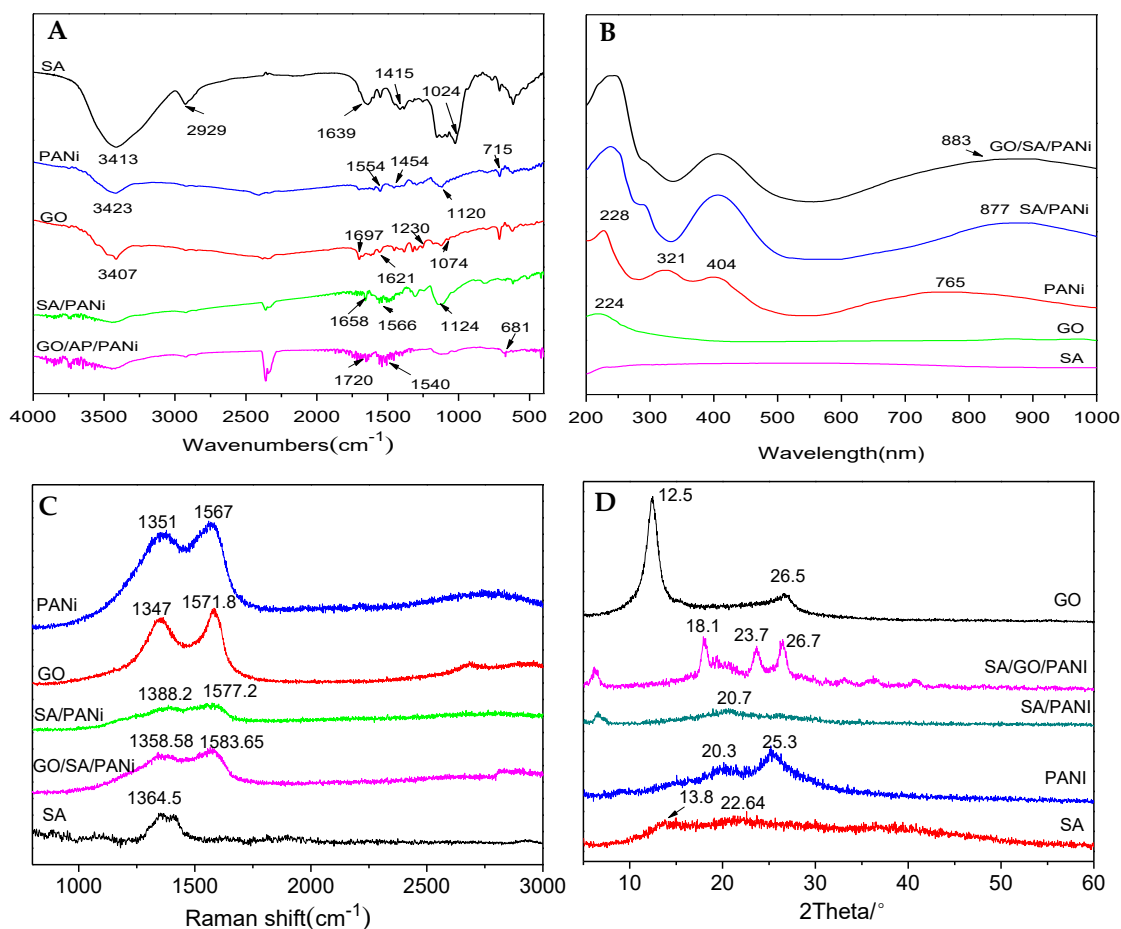


Figure 2. (A) FTIR spectra, (B) UV-vis absorption spectra, (C) Raman spectra and (D) XRD patterns of SA, GO, PANi, SA/PANi and GO/SA/PANi.

In addition, an abroad peak centered at 26.7° was attributed to weak stacking between GO sheets. The two weak peaks of 13.8° and 22.6° were typical diffraction peaks of SA. The characteristic peaks of 20.3° and 25.3° were attributed to the periodic vertical and horizontal alignment of the PANi molecular chain. The characteristic peak of 20.7° in SA/PANi was attributed to PANi, and this peak became wider comparing to pure PANi. The XRD spectrum of GO/SA/PANi showed three characteristic bands at 18.1° , 23.7° and 26.5° , indicating that the PANi in hybrids was partially crystalline [28-29]. These results

confirmed the formation of GO/SA/PANi hydrogel, in which the macromolecule interactions between SA, GO and PANi chains were formed.

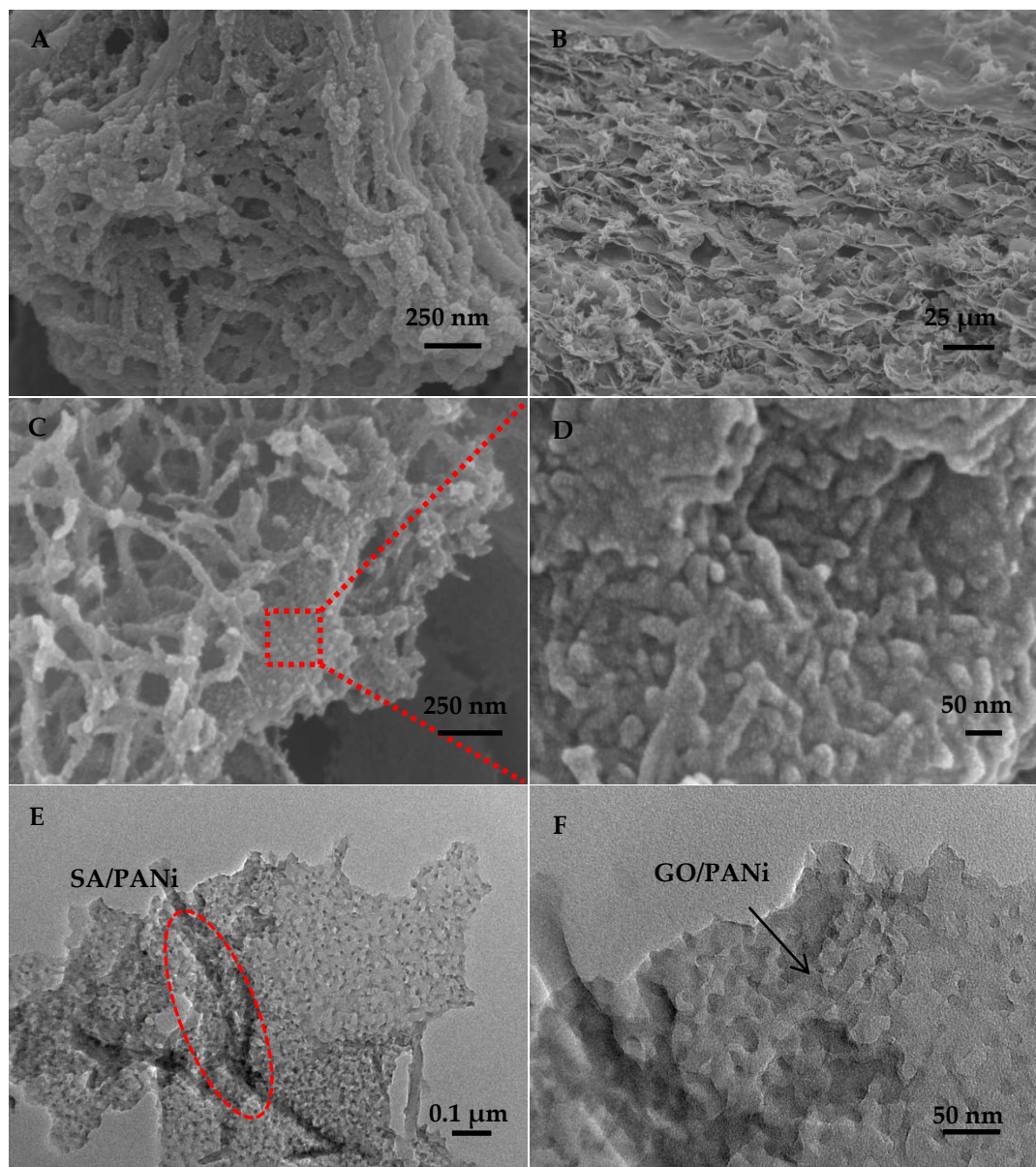


Figure 3. (A) SEM image of SA/PANi hydrogel; (B) SEM image of GO/SA/PANi hydrogel; (C) and (D) are SEM images of GO/SA/PANi hydrogel at different magnifications. (E) and (F) TEM images of GO/SA/PANi with different magnifications.

The micro-structure of hydrogels were examined and compared by the SEM images as shown in Figure 3. As shown in Figure 3A, fibers were obviously observed, which was similar with previous works [30]. The fibers were due to assemble of PANi entangle with the SA chains. After introduction of GO, it was found that the microscopic morphology was a 3D network structure based on the layers interact with fibrous substances as shown in Figure 3B. This phenomenon was attributed to the interaction between PANi and SA (or GO) [22]. At higher magnification (in Figure 3C), it clearly showed that some fibers were coated on surface of GO nano-sheets. The morphology and size of fibers

was similar with SA/PANi fibers as shown in Figure 3A. Yet, the size of fibers grown on GO layer (in Figure 3D) was smaller than that of pure SA/PANi fibers. The micro-structure of GO/SA/PANi was further examined by TEM images as shown in Figure 3E and 3F. Figure 3E clearly showed GO sheet combination with SA/PANi fibers, and the GO sheet was covered with PANi as shown in Figure 3F. Due to the presence of SA/PANi nano-fiber structure, there have no direct contact between GO/PANi laminar structures. This prevented the adsorption and agglomeration between the GO/PANi nano-sheets [31], providing more access for the hydrogel structure.

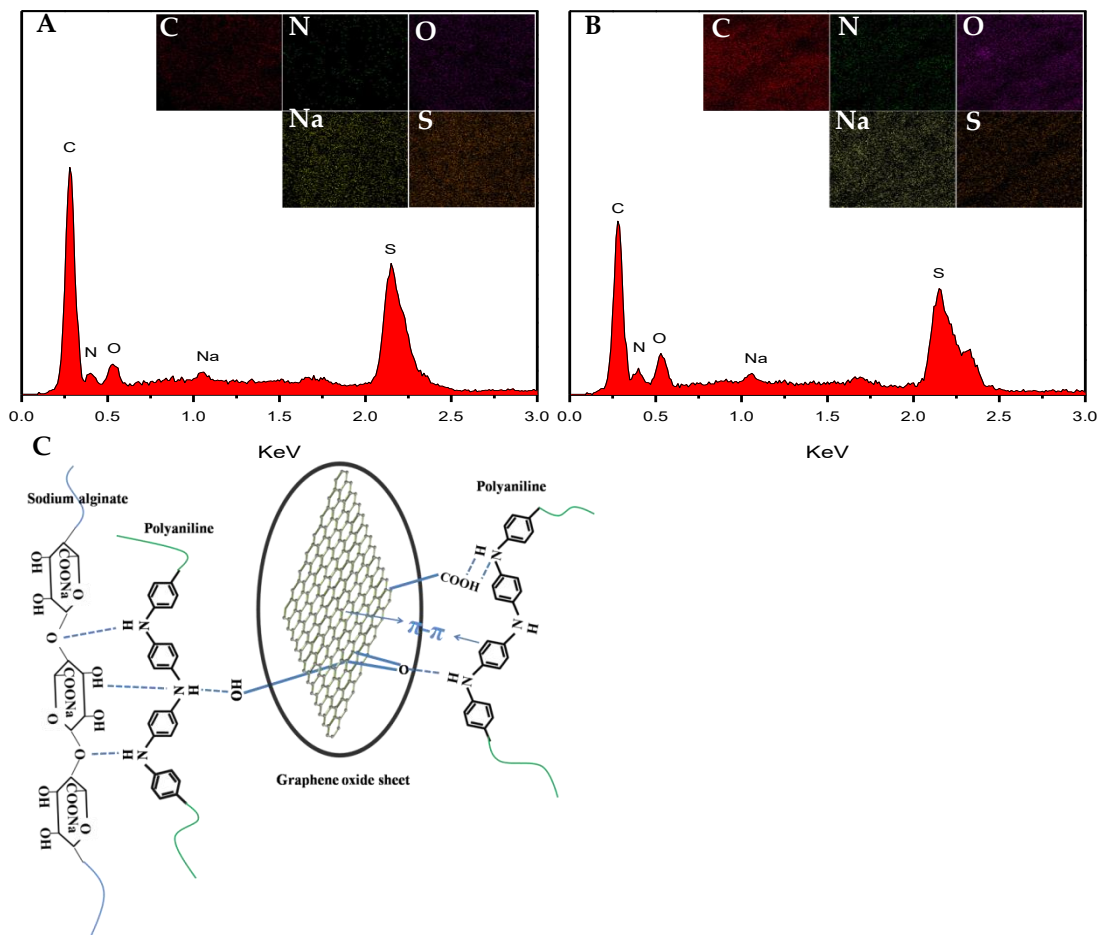


Figure 4. (A) and (B) are EDS spectrums of SA/PANi and GO/SA/PANi hydrogels (Insert the elemental mapping images); (C) Schematic illustration of possible molecular interaction in GO/SA/PANi hydrogel.

The elemental mapping images and energy-dispersive X-ray diffraction (EDS) of SA/PANi and GO/SA/PANi hydrogels were shown in Figure 4. The elemental mapping images clearly presented C, O, N, S and Na in hydrogel and clearly revealed that these elements were uniformly distributed in the hydrogels as shown in inset of Figure 4. In addition, these C, O, N, S and Na elements could be clearly observed in EDS spectra. The content of C, O, N, S and Na in SA/PANi hydrogel were calculated to be 61.4wt%, 14.9wt%, 12.6wt%, 9.5wt% and 1.6wt%, respectively. The content of C, O, N, S and Na in

GO/SA/PANi hydrogel were calculated to be 49.5wt%, 17.8wt%, 16.2wt%, 14.8wt% and 1.7wt%, respectively. Obviously, the N content of GO/SA/PANi hydrogel (ca. 16.2wt%) was higher than the N content (ca. 12.6wt%) of SA/PANi hydrogel. It further confirmed the successful preparation of GO/SA/PANi based on SA, GO and PANi with high purity and that the GO sheets could fix PANi, and increased the content of PANi in GO/SA/PANi hydrogel. Regarding above results, the possible interactions between the various macromolecules in GO/SA/PANi hydrogel were illustrated in Figure 4C. There have formed strong hydrogen bond and π - π interaction between PANi with SA and PANi with GO, which attributed to the -NH- and benzene rings in PANi.

After in-situ polymerization of aniline, PANi fibers could be easily introduced into the cross-linked network of SA/PANi and GO/SA/PANi hydrogels. The PANi fiber could effectively improve the electrical conductivity of SA/PANi and GO/SA/PANi hydrogels. As shown in Table 1, the electricity conductivity of the SA/PANi and GO/SA/PANi hydrogels were about 15.2 S/m and 16.8 S/m, respectively. After immersing in the 1.0 M H₂SO₄ aqueous solution, the conductivity of SA/PANi and GO/SA/PANi hydrogels increased rapidly to 204.4 S/m and 210.4 S/m. This indicated that during the immersing process, H₂SO₄ have permeated into the cross-linked network of SA/PANi and GO/SA/PANi hydrogels. To illustrate the electricity conductivity, the conductive phenomenon was also shown directly in Figure 5. From Figure 5, it could be seen that the SA/PANi and GO/SA/PANi hydrogels could conduct electricity well. The large conductivity of present hydrogel was attributed to that there was no exposed non-conductive polymer material in the structure.

Table 1. Electrical conductivity of the SA/PANi and GO/SA/PANi hydrogels.

Sample		U (V)	I (mA)	δ (S/m)
SA/PANi	water	0.0234	0.484	15.2
	1.0 M H ₂ SO ₄	0.0047	1.315	204.4
GO/SA/PANi	water	0.0206	0.469	16.8
	1.0 M H ₂ SO ₄	0.0084	2.414	210.4

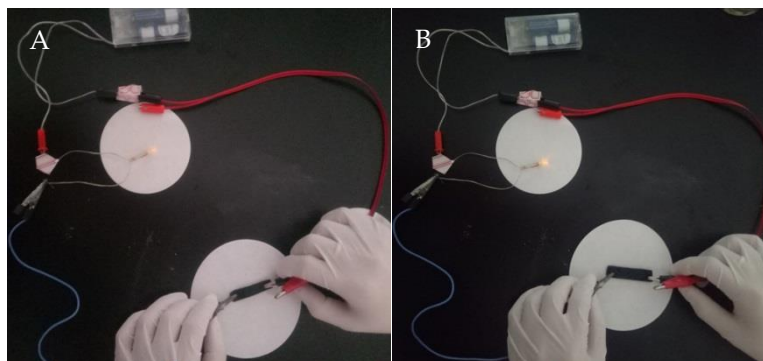


Figure 5. The conductivity photos of (A) SA/PANi hydrogel and (B) GO/SA/PANi hydrogel.

Figure 6A shows the impedance plot of SA/PANi and GO/SA/PANi hydrogel. As shown in Figure 6A, the impedance plot was consisted of a semicircle in the high-to-medium frequency region arising from the chemical reaction process [32]. At high frequency (close to 100.0 kHz), the equivalent

series resistance (R_{ESR}) of SA/PANi and GO/SA/PANi hydrogel obtained from the first intersection with the real axis was about 5.8Ω and 3.4Ω , respectively. The result indicated a low internal resistance for GO/SA/PANi hydrogel electrodes, which was consistent with high electrical conductivity of GO/SA/PANi hydrogel. The impedance plot of both electrodes in the area of high frequencies showed a typical semicircle, and the diameter of this semicircle corresponded to the charge-transfer resistance (R_{ct}) of ion diffusion in the electrode material [33-34]. The R_{ct} of SA/PANi and GO/SA/PANi hydrogel was about 4.9Ω and 3.1Ω , respectively. Comparing to SA/PANi hydrogel, the GO/SA/PANi hydrogel provided more diffusion paths from electrolyte to electrodes. Furthermore, the straight lines in the area of low frequencies corresponded to a pure capacitance behavior. The slope of the straight line for GO/SA/PANi hydrogel was larger than that of SA/PANi hydrogel, indicating a more ideal capacitance behavior. These results further indicated that GO/SA/PANi hydrogels could be favorable candidates as electrode materials for supercapacitors. In addition, according to above results, the equivalent circuit of GO/SA/PANi hydrogel electrode was proposed as shown in Figure 6B. It involved the following elements: the bulk solution resistance (R_s), the charge transfer resistance (R_{ct}), the contact resistance (R_c), and a Warburg diffusion element attributable to the diffusion of ions. In addition, C_L in the circuit model represented the combination of the double-layer capacitance from carbon substrate and the pseudo capacitance (C_F) from PANi, which was related to its redox transition. Obviously, the GO/SA/PANi hydrogel supercapacitor exhibited lower R_{ESR} and R_{ct} values than SA/PANi hydrogel supercapacitor. Furthermore, impedance performance of GO/SA/PANi hydrogel supercapacitor was also lower than previously reported RGO/PANi composites (non-hydrogel) supercapacitor [10,19]. And, all of these results owing to its ideal conductive network structure.

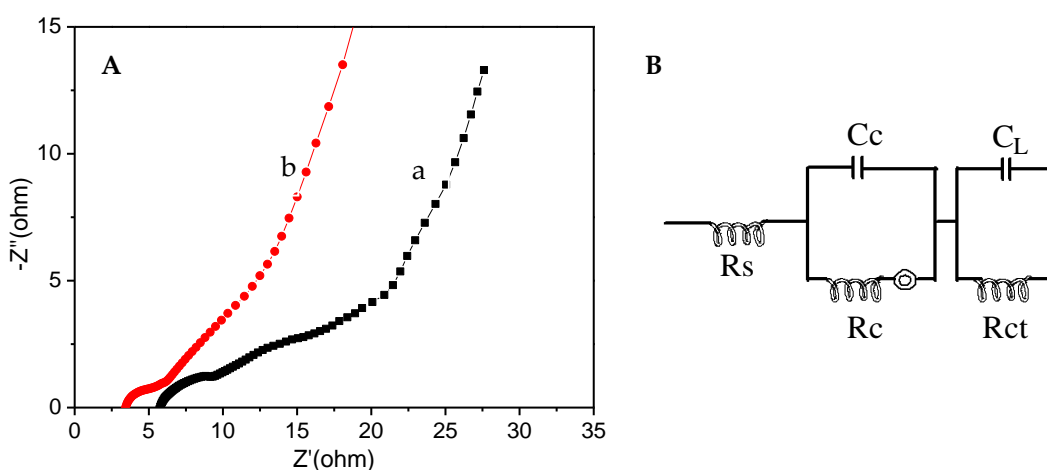


Figure 6. (A) The impedance spectra of (a) SA/PANi and (b) GO/SA/PANi hydrogel, (B) Equivalent circuit for simulating the impedance spectra of the GO/SA/PANi hydrogel electrode.

Figure 7 shows the CV curves of supercapacitors based on SA/PANi and GO/SA/PANi hydrogels as function of scan rates. All CV curves exhibited nearly rectangular and symmetrical shape. In addition, the current response increased with increasing in the scan rate. When the scan rate was about 100 mV/s , the CV curve window area of GO/SA/PANi hydrogel was larger than that of SA/PANi hydrogel. Due to the specific capacitance of supercapacitor was directly proportional to the area of its

CV, the result suggested that the specific capacitance of supercapacitor based on GO/SA/PANi hydrogel was larger than that of supercapacitor based on SA/PANi hydrogel. This was due to the presence of more PANi for GO/SA/PANi hydrogel, providing larger active surface area for charge accumulation comparing to SA/PANi hydrogel.

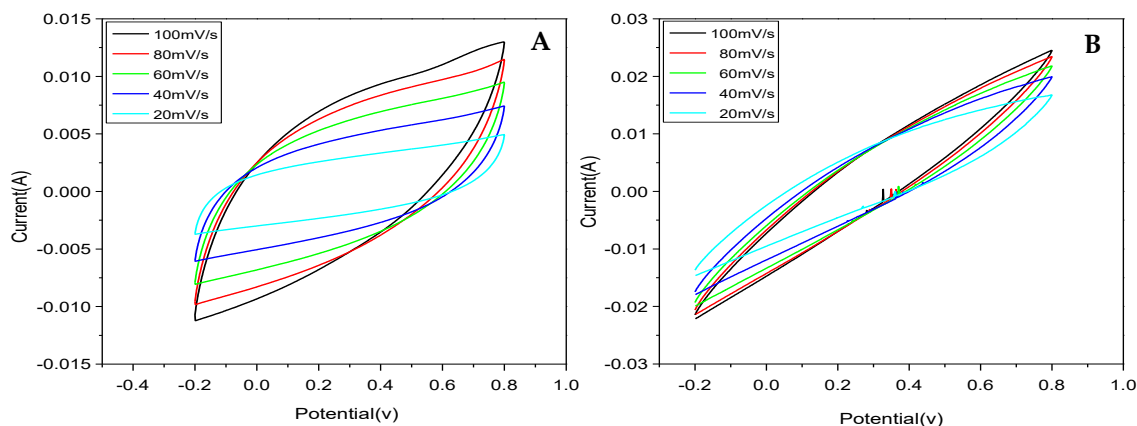


Figure 7. CV plot of supercapacitor based on (A) SA/PANi and (B) SA/GO/PANi at various scan rates of 20.0 mV/s, 40.0 mV/s, 60.0 mV/s, 80.0 mV/s and 100.0 mV/s.

Figure 8A shows the GCD curves of supercapacitors based on SA/PANi and SA/GO/PANi hydrogels at current density of 1.0 mA/cm². It was found that the discharge time of the supercapacitor based on GO/SA/PANi hydrogel was obviously longer to the supercapacitor based on SA/PANi hydrogel. This result further indicated that the supercapacitor based on GO/SA/PANi hydrogel possessed larger capacitance comparing to supercapacitor based on SA/PANi hydrogel. Yet, an IR-drop was clearly observed for the supercapacitors based on SA/PANi and SA/GO/PANi hydrogels. According to above results of conductivity and EIS, the IR-drop may be attributed to the resistance of ion transport and diffusion between diaphragm and electrolyte. The IR-drop can be reduced by the optimization of diaphragm structure. The rate performance of the supercapacitor based on GO/SA/PANi hydrogel was also evaluated by charging/discharging at different current densities as shown in Figure 8B. This supercapacitor could maintain its triangular charge/discharge curves when the current density was reduced from 2.5 to 0.5 mA/cm², indicating rapid charge propagation. The highest area-normalized capacitance or gravimetric capacitance was found to be 2.3 F/cm² or 779.9 F/g at current density of 0.5 mA/cm². As shown in Figure 8C, the presented all-solid-state supercapacitor device showed a relatively poor rate capability. However, it still showed larger specific capacitance than some supercapacitors based on other conductive hydrogels [21, 26, 35-36]. Furthermore, the specific capacitance of supercapacitor based on GO and PANi reported in present and previous works were also concluded and compared as shown in Table 2 [12, 15-16, 28, 30]. It was also clearly observed that the supercapacitor based on present GO/SA/PANi hydrogel showed highest capacitance comparing to previously reported GO/PANi-based materials. The result was attributed to good conductivity and 3D porous structure of GO/SA/PANi hydrogel.

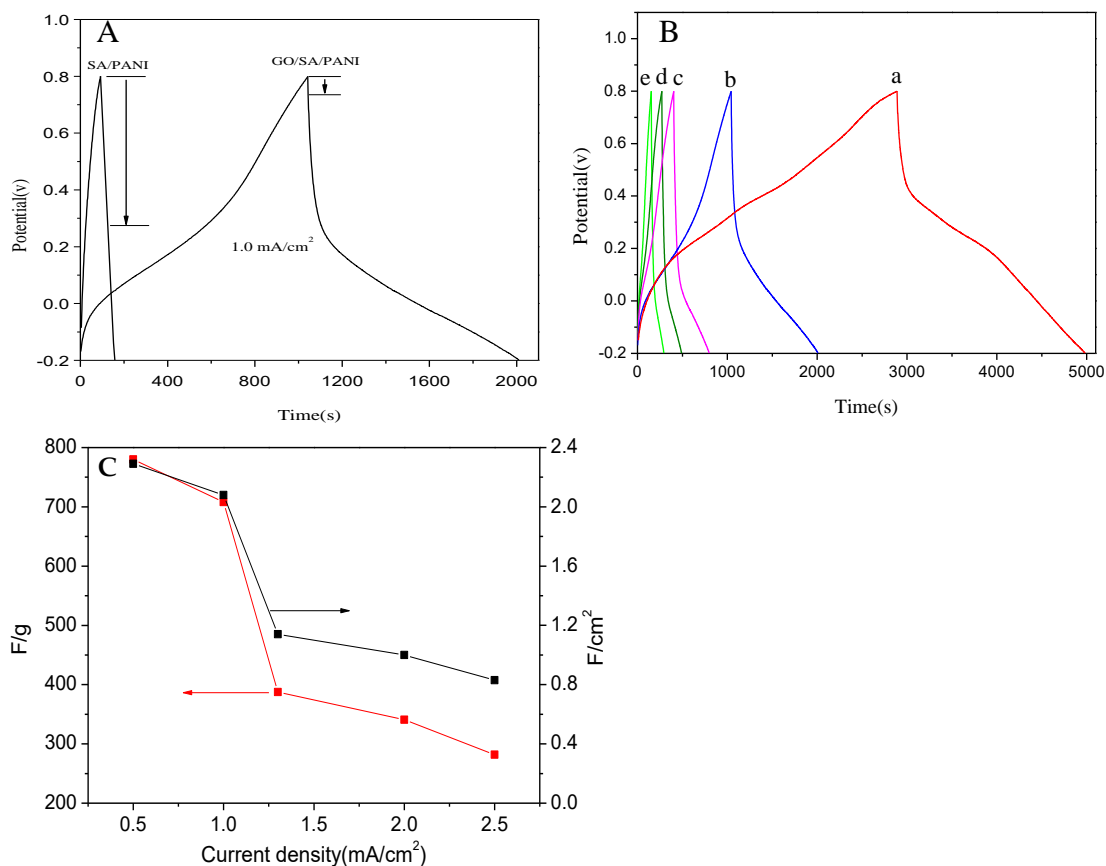


Figure 8. (A) GCD curves of the SA/PANi and GO/SA/PANi supercapacitors at current density of 1.0 mA/cm². (B) GCD curves of the GOSAP supercapacitor at current densities of (a) 0.5 mA/cm², (b) 1.0 mA/cm², (c) 1.3 mA/cm², (d) 2.0 mA/cm² and (e) 2.5 mA/cm². (C) Specific capacitance of the GO/SA/PANi supercapacitor at varied GCD current densities.

Table 2. Data of previous GO/PANi-based reports compared with our work.

S.No.	Composite materials	Hydrogel(Yes/No)	C _m (F/g)	Reference
1.	GO/PANi	No	555	[16]
2.	rGO/PANi	No	385	[28]
3.	GO/PANi/Co(O) ₂	No	723	[12]
4.	GO/PA/PPD/PAi	Yes	610	[30]
5.	GO/SA/PANi	Yes	780	This work

Note: PA: phytic acid; PPD: p-phenylenediamine.

As well-known, electrochemical stability is an important parameter for the application of supercapacitors. In general, conducting hydrogels showed poor cycling stabilities due to easily expand and shrink during charge/discharge.

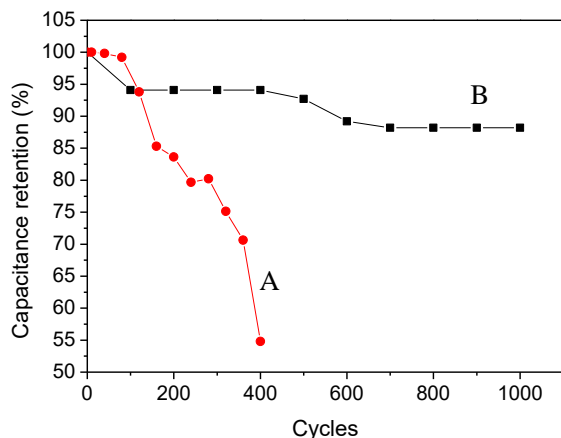


Figure 9. Cycling stability of supercapacitor based on (A) SA/PANi and (B) GO/SA/PANi hydrogel at current density of 1.0 mA/cm^2 .

Therefore, their mechanical stability and capacitance was obviously reduced after a certain cycles of charge/discharge process. As shown in Figure 9A, the supercapacitor based on SA/PANi hydrogel only maintained 54.8% of the initial capacitance after 400 cycles. In a comparison, the supercapacitor based on GO/SA/PANi hydrogel maintained 88.2% of the initial capacitance after 1000 cycles as shown in Figure 9B. The better cycling stability of GO/SA/PANi was attributed to the synergistic effects between SA, PANi and GO comparing to SA/PANi hydrogel. The GO nano-sheet can effectively enhance the mechanical stability during charge/discharge process, resulting in higher specific capacitance and cycle stability. It revealed the significance of morphological control in PANi/polymer hybrids, which could be realized simply by the structural design of functional groups on GO.

4. CONCLUSIONS

In summary, the GO/SA/PANi hydrogel was prepared via simple approach at room temperature. This work demonstrates a novel multi-structural network design strategy for the mechanical enhancement in GO/SA-based conducting hydrogel. This unique architecture provided efficient and rapid pathways for ion diffusion as well as improved cycling stability. The electrochemical studies showed that GO/SA/PANi hydrogel possessed a high specific capacitance and cycling stability for supercapacitor electrodes. This research provides a safe, cheap and easy approach to prepare high-ionic conductivities hydrogel for the application of supercapacitors.

References

1. J.F. Sun, Y. Huang, Y.N.S. Sea, Q. Xue, Z.F. Wang, M.S. Zhu, H.F. Li, X.M. Tao, C.Y. Zhi, H. Hu, *Mater. Today Energy*, 5 (2017) 1.
2. G.J. Rydzek, Q.M. Li, M. Schaaf, P. Hill, J.P. Boulmedais, F. Ariga, *Nano Today*, 10 (2015) 138.
3. J.H. Yu, F.F. Xie, Z.C. Wu, T. Huang, J.F. Wu, D.D. Yan, C.Q. Huang, L. Li, *Electrochim. Acta*, 259 (2018) 968.

4. S.P. Xin, Y.R. Kang, S.X. Qu, S.S. Han, *Mater. Lett.*, 175 (2016) 126.
5. H.X. Wang, D. Liu, X.J. Duan, P.C. Du, J.S. Guo, P. Liu, *Mater. Design*, 108 (2016) 801.
6. N.P. Shetti, D.S. Nayak, S.J. Malode, R.M. Kulkarni, D.B. Kulkarni, R.A. Teggi, V.V. Joshi, *Surf. Interfaces*, 9 (2017) 107.
7. S.J. Lee, Y.R. Lim, S. Ji, S.K. Kim, Y. Yoon, W. Song, S. Myung, J. Lim, K.S. An, J.S. Park, S.S. Lee, *Carbon*, 126 (2018) 241.
8. N. Batisse, E. Raymundo-Pinero, *J. Power Sources*, 348 (2017) 168.
9. W.W. Li, F.X. Gao, X.Q. Wang, *Angew. Chem., Int. Ed.*, 55 (2016) 1.
10. D. Liu, H.X. Wang, P.C. Du, W.L. Wei, Q. Wang, P. Liu, *Electrochim. Acta*, 259 (2018) 161.
11. Z.H. Luo, L.H. Zhu, H.Y. Zhang, H.Q. Tang, *Mater. Chem. Phys.*, 139 (2013) 572.
12. L. Ma, L.J. Su, J. Zhang, D.Y. Zhao, C.L. Qin, Z. Jin, K. Zhao, *J. Electroanal. Chem.*, 777 (2016) 75.
13. X.Q. Yan, J. Yang, F. Chen, L. Zhu, Z.Q. Tang, G. Qin, Q. Chen, G.M. Chen, *Compos. Sci. Technol.*, 163 (2018) 81.
14. A. Kumar, K.M. Rao, S.S. Han, *Carbohydr. Polym.*, 193 (2018) 228.
15. H.B. Huang, X.P. Zeng, W. Li, H. Wang, Q. Wang, Y.J. Yang, *J. Mater. Chem. A*, 2 (2014) 16516.
16. J.J. Xu, K. Wang, S.Z. Zu, B.H. Han, Z.X. Wei, *ACS. nano*, 9 (2010) 5019.
17. J.W. Jeon, S.R. Kwon, L. Jodie, *J. Mater. Chem. A*, 7 (2015) 3757.
18. H.T. Yu, X. Ge, C. Bulin, R.G. Xing, R.H. Li, G.X. Xin, B.W. Zhang, *Electrochim. Acta*, 253 (2017) 239.
19. P. Lv, X. Tang, R.L. Zheng, X.B. Ma, K.H. Yu, W. Wei, *Nanoscal. Res. Lett.*, 12 (2017) 1.
20. H.N. Van, L.L. Tang, J.J. Shim, *Colloid Polym. Sci.*, 291 (2013) 2237.
21. Q. Zhao, J.H. Chen, F.B. Luo, L. Shen, Y. Wang, K. Wu, M.G. Lu, *J. Appl. Polym. Sci.*, 44808 (2017) 1.
22. Q. Wang, J.L. Li, F. Gao, W.S. Li, K.Z. Wu, X.D. Wang, *New Carbon Mater.*, 23 (2008) 275.
23. L.M. da Silva, D.A. Almeida, S.S. Oishi, *Mat. Sci. Eng. B*, 228 (2018) 249.
24. J.M. Liu, K. Zhu, T.F. Jiao, R.R. Xing, H. Wei, L.X. Zhang, Q.R. Zhang, Q.M. Peng, *Colloids Surf. A*, 529 (2017) 668.
25. A. Rose, K.G. Prasad, T. Sakthivel, V. Gunasekaran, T. Maiyalagan, T. Vijayakumar, *Appl. Surf. Sci.*, 449 (2018) 551.
26. D.D. Xu, Q. Xu, K.X. Wang, J. Chen, Z.M. Chen, *ACS Appl. Mater. Interfaces*, 6 (2014) 200.
27. P.C. Du, H.C. Liu, C. Yi, K. Wang, X. Gong, *ACS Appl. Mater. Interfaces*, 7 (2015) 23932.
28. Q. Zhao, J.H. Chen, F.B. Luo, L. Shen, Y. Wang, K. Wua, M.G. Lu, *Synth. Met.*, 221 (2016) 103.
29. F.Y. Ke, Y. Liu, H.Y. Xu, Y. Ma, S.Y. Guang, F.Y. Zhang, N.B. Lin, M.D. Ye, Y.H. Lin, X.Y. Liu, *Compos. Sci. Technol.*, 142 (2017) 286.
30. J.W. Luo, W.B. Zhong, Y.B. Zou, C.L. Xiong, W.T. Yang, *J. Power Sources*, 319 (2016) 73.
31. D.Q. Liu, Z. Jia, J.X. Zhu, D.L. Wang, *J. Mater. Chem. A*, 3 (2015) 12653.
32. X. Fan, W.L. Chen, S.H. Pang, W. Lu, Y. Zhao, Z. Liu, D. Fang, *Chem. Phys. Lett.*, 689 (2017) 162.
33. Y.W. Huang, M. Zeng, J.B. Chen, Y.Q. Wang, Q.Y. Xu, *Mater. Design*, 148 (2018) 104.
34. X.X. Wang, M. Xu, Y.L. Fu, S.Y. Wang, T. Yang, K. Jiao, *Electrochim. Acta*, 222 (2016) 701.
35. Y.T. Tan, Y.F. Zhang, L.B. Kong, F. Ran, *J. Alloy Compd*, 722 (2017) 1.
36. W. Liu, S. Wang, Q. Wu, L. Huan, X. Zhang, C. Yao, M. Chen, *Chem. Eng. Sci.*, 156 (2016) 178.